Ocean Modelling 202 (2026) 102735

Contents lists available at ScienceDirect

Ocean Modelling

journal homepage: www.elsevier.com/locate/ocemod

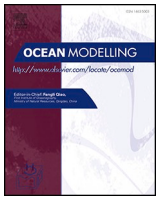

On the application of the two-time stepping Euler forward Runge-Kutta schemes to the shallow water equations: Global truncation error, numerical viscosity, consistency, energy conservation, inertial stability and phase error

Jia Wang [a,*], David Cannon [b], Yang Song [b], Haoguo Hu [b], Ayumi Fujisaki-Manome [b,c], Andrea VanderWoude [a], Oliver Fringer [d]

[a] NOAA Great Lakes Environmental Research Laboratory, Ann Arbor, MI, USA
[b] Cooperative Institute for Great Lakes Research, University of Michigan, Ann Arbor, MI, USA
[c] Department of Climate and Space Sciences and Engineering, University of Michigan, Ann Arbor, MI, USA
[d] Department of Engineering, Stanford University, Palo Alto, CA, USA

ARTICLE INFO

Keywords:
Runge-Kutta scheme
Predictor-corrector scheme
Numerical viscosity
Inertial stability
Phase speed
Global/local truncation error
Consistency
Energy conserving
Model drifting
Bias correction

ABSTRACT

This study aims to investigate several issues relating to the application of Runge-Kutta (RK) schemes, which are popularly applied to single-variable ordinary differential equations (ODEs) and multi-variable partial differential equations (PDEs), such as shallow water equations (SWEs). Starting with the original mathematical definition of the RK scheme, it was found that RK schemes are fundamentally similar to the first-order Euler forward predictor-corrector (PC) scheme. It is shown that 2-time stepping RK and other schemes actually are the PC schemes. Truncation error analysis shows that the 2-, 3-, and 4-stage PC/RK (or PC2/RK2, PC3/RK3, and PC4/RK4, respectively) are of first-order accuracy in time due to the nature of the first-order Euler forward scheme at each stage. Truncation analysis shows that 1st-order PC/RK schemes discard the physically-based bi-harmonic viscosity term. This is equivalent to adding the same, but a negative viscosity to the numerical scheme, and is inconsistent with their original PDEs if compared to the 2nd-order accurate leapfrog scheme. It is shown that each step of the multi-stage PC (i.e., RK) iterative process improves the precision of its previous stage in terms of amplification factor and phase speed. Using a pure advection system, it is proven that any 1st-order Euler forward scheme in time and space cannot conserve energy. It is also confirmed that the explicit treatment of unweighted and equally-wighted Coriolis terms in PC/RK schemes produce inertial instability, which must be dampened using numerical filters or by adding unrealistically high viscosity. As a result, models that use such schemes are overly-damping, leading to smoothing of important dynamical processes, such as mesoscale eddies, vertical stratification, and the strength of horizontal fronts. Three types of 3-stepping (at *n-1, n, n + 1*, leapfrog-like) schemes are investigated including the leapfrog-trapezoidal scheme, Adams-Bashforth scheme, and leapfrog-hoRA (high order Robert-Asselin) filter scheme. It is found that the leapfrog-hoRA scheme is advantageous in that 1) it is of second-order accuracy in general, and can be configured to achieve third-order accuracy when β=0.4, 2) it introduces no numerical viscosity, and 3) it produces nearly neutral inertial stability in terms of both amplification factor and phase speed.

1. Introduction

Numerical community ocean and atmospheric models are widely available for users to apply to environmental research, simulation, and forecasting. For these models that solve parabolic partial differential equations (PDEs) such as shallow water equations (SWEs) in a rotating plane, time and space are discretized. To handle temporal discretization for time integration schemes, conventional finite differencing methods, like the 3-time stepping ($n + 1, n, n\text{-}1$) leapfrog scheme are used and more and more 2-time stepping ($n + 1, n$) methods are used, which were

* Corresponding author.
E-mail address: jia.wang@noaa.gov (J. Wang).

https://doi.org/10.1016/j.ocemod.2026.102735
Received 14 March 2025; Received in revised form 2 December 2025; Accepted 31 March 2026
Available online 14 April 2026
1463-5003/Published by Elsevier Ltd.

widely employed for solving ordinary differential equations (ODEs). Runge-Kutta (RK) and Adams-Bashforth (A-B) schemes are some of the popular 2-time stepping methods applied to geophysical fluid dynamics (GFD) models to solve parabolic partial differential equations (PDEs) such as the rotational form of the shallow water equations (SWEs). For example, 3-stage RK schemes (RK3) are used in both the Finite-Volume Community Ocean Model (FVCOM; Chen et al., 2013) and the Weather Research and Forecasting model (WRF; Skamarock et al. 2019; Wicker and Skamarock, 2002) to simulate ocean and atmospheric dynamics, respectively. A 2-stage RK (or called Euler forward-backward) scheme is also used for time integration in MOM6 (Modular Ocean Model version 6; https://mom6.readthedocs.io/en/main/api/generated/modules/mom.html), which replaces the previously utilized leapfrog scheme in the older version of MOM.

In the newer version of ROMS (the regional ocean modeling system), the barotropic mode is stepped with a 3-stage leapfrog-Adams-Moulton scheme with forward-backward feedback. The baroclinic mode is stepped with a 3-stage Adams-Bashforth scheme. Tracers are stepped with a 2-stage leapfrog scheme with a trapezoidal corrector. Details of the time-stepping schemes are found in Shchepetkin and McWilliams (2009). Schlichting et al. (2024) found that a "negative numerical viscosity" exists in the simulation of the coastal front using ROMS. Numerical mixing due to the discretization of tracer advection (Klingbeil et al. 2014; Homes et al. 2021) is quantified for three advection schemes in idealized numerical simulations and mixing in frontal zones is dominated by numerical mixing over the physical mixing even at sub-mesoscale-resolving resolutions, which seriously suppresses (sub-) mesoscale eddies, and frontal structure.

Although the FVCOM is widely used in both research and operational models around the globe, Wang et al. (2023) found that the numerical damping produced by default Euler forward RK schemes results in overly-diffuse temperature stratification. This damping was linked to i) inertial instability, which can only be dampened using very small-time steps and unrealistically large viscosity, leading to smearing (or smoothing) of the thermal structure; and ii) the first order accuracy of the Euler forward scheme, which results in "drifting" of the numerical solution over time.

In a number of applications of the WRF model (Skamarock et al. 2019), it has been reported that WRF-simulated results are quite dissipative, so much so that nudging to observations is required to produce reasonable simulations (Hutson et al. 2024). In some recent studies of downscaled future climate scenarios, models were run in 20-year windows (e.g. hindcast, mid-century, and end-century; Zobel et al. 2018). While these shorter simulations are sometimes justified by computational resources, they also help alleviate issues caused by model drift that occurs over longer simulation periods, as reported by Bruyère et al. (2014) and Dosio and Paruolo (2011).

To correct large model drifting caused by discretized numerical schemes, physical parameterizations, and forcing biases, a "bias correction" method is widely being used to correct the simulations using observations and assimilated model reanalysis products (Bruyère et al. 2014). This bias-correction method is used not only for hindcast simulations, but also for future climate projections (Dosio and Paruolo, 2011) and is often justified with a simple rationale that all numerical models introduce errors anyway. Our argument is that although bias-correction is an effective way to bring a drifting model back to the expected observations or reanalysis products (e.g., treating the symptoms), it ignores the root causes of the errors (e.g., the disease). We further argue that the bias-correction should be used only after the biases resulting from numerical schemes, physical processes, and/or parameterizations have been identified and corrected.

It should be addressed that the fundamental differences between ordinary fluid mechanics (OFM) and geophysical fluid dynamics (GFD) in the ocean and atmosphere are 1) rotation and 2) stratification (implicitly means low viscosity), which form the core scientific topics of GFD (Pedlosky, 1979; Holton 1979). Therefore, finite differencing schemes in ocean or atmospheric models need to preserve these two fundamental physical properties of the continuum medium. This requires finite differencing schemes in a model to (i) retain a neutral inertial stability [i.e., the eigenvalue λ or the amplification factor (AF) need to be on the unit circle $|\lambda|=1$ for the inertial mode; Wang and Ikeda 1997a, Durran 2010; Wang et al. 2023]; (ii) maintain the non-dispersive property of the inertial frequency, f (Wang 1996; Beckers 1999; Beckers and Deleersnijder 1993); and (iii) introduce no numerical viscosity (in the low-viscous ocean) in order to preserve vertical stratification, horizontal (frontal) structure, mesoscale and sub-mesoscale eddies (Wang and Ikeda 1997b; Schlichting et al. (2024).

It is also noted that baroclinic Rossby radii of deformation in the ocean (Chelton et al. 1998), which range from ~100 km at the equator to ~10 km at 50 N, and even a few kilometers in the Arctic seas (Nurser and Bacon 2014), are one magnitude of smaller than in the atmosphere at any latitude due to much stronger and more permanent vertical stratification in the ocean (Gill 1982). This implies that the inertial mode in the ocean is more important than in the atmosphere, and that the numerical schemes used in the ocean, where vertical and horizontal resolutions are higher, should be more sophisticated to retain the non-dispersive inertial mode. On the other hand, the atmosphere, similar to fresh water lakes (Bai et al., 2013; Cannon et al. 2023, 2024), has much weaker stratification because density depends primarily on temperature. As a result, these systems often experience deep vertical convection that zeros out any previously-cumulated computational errors/bias in vertical stratification. However, in the permanent, strong-stratified ocean, where salinity plays a major role in density stratification, the computational error would be cumulated and compounded in both the vertical and horizontal domain. Therefore, finite differencing schemes in an ocean model should be more carefully designed, because numerical schemes widely used for ODEs and atmospheric GFD models may not be suitable for strong-stratified and strongly-rotating (much smaller baroclinic Rossby radii of deformation) ocean modeling.

The explicit objective of this study is to explore the suitability of widely-used PC/RK schemes time integration for strong non-linear ODEs as applied for f-plane shallow water equations in ocean and atmospheric models. In doing so, we investigate the disadvantages of RK schemes in their application to SWEs, especially as compared to the widely-used leapfrog scheme. Consequently, remedies are provided to cure the problems from the root causes, rather than treating the symptoms by adding filters, increasing the viscosity to dampen existing instabilities, or by using bias-correction (i.e., data nudging) to forcefully bring the drifting model back to measurements.

In Section 2, the conventional finite differencing scheme using Taylor expansion only and the RK scheme using both Taylor series expansion and an iterative (PC) derivative method to improve the precision are investigated. The similarity between the RK schemes and PC schemes is also revealed to confirm that RK schemes are in the same family as the PC framework. In Section 3, the similarity and differences between the RK approximation and conventional finite differencing approximation are shown. In Section 4, using PC as a proxy for RK, analyses of the truncation error, consistency, and energy conserving properties are conducted. In Section 5, three types of 3-time stepping (leapfrog-like) schemes that are widely used and their inertial stability and phase errors properties are investigated and compared. Finally, Section 6 provides conclusions including recommendation and in-depth discussion.

2. Runge-Kutta (RK) methods for non-linear ODEs

Runge-Kutta methods are widely used to numerically solve non-linear ordinary differential equations (ODEs) in the following initial problem (Li and Feng, 1990)

$$\begin{cases} \dfrac{du(t)}{dt} = F(u,t), \\ u(t_0) = u_0 \end{cases} \tag{1}$$

where $F(u, t)$ is the non-linear function of both u and t. Using Taylor series expansion, we have

$$\mathrm{u}(\mathrm{t}_1) = \mathrm{u}(\mathrm{t}_0) + \frac{\Delta t}{1!}\frac{du}{dt} + \frac{\Delta t^2}{2!}\frac{d^2u}{dt^2} + \frac{\Delta t^3}{3!}\frac{d^3u}{dt^3} + \ldots + \frac{\Delta t^p}{p!}\frac{d^pu}{dt^p} + O\left(\Delta t^{p+1}\right)$$

$$= \mathrm{u}(\mathrm{t}_0) + \frac{\Delta t}{1!}F + \frac{\Delta t^2}{2!}F' + \frac{\Delta t^3}{3!}F'' + \ldots + \frac{\Delta t^p}{p!}F^{p-1} + O(\Delta t^p) \tag{2}$$

while the conventional finite differencing approximation is shown as

$$\frac{du}{dt} = \frac{\mathrm{u}(\mathrm{t}_1) - \mathrm{u}(\mathrm{t}_0)}{\Delta t} - \frac{\Delta t^1}{2!}\frac{d^2u}{dt^2} - \frac{\Delta t^2}{3!}\frac{d^3u}{dt^3} - \cdots + \frac{\Delta t^{p-1}}{p!}\frac{d^pu}{dt^p} + O(\Delta t^p)$$

$$\approx \frac{\mathrm{u}(\mathrm{t}_1) - \mathrm{u}(\mathrm{t}_0)}{\Delta t} + O(\Delta t) \tag{2′}$$

where $u(t_0)=u_0$, $u'=\frac{du}{dt}=F[u(t_0), t_0]=F(u_0, t_0)$, and the prime is the total derivative. Then we have the following partial derivatives ($F_t = \partial F/\partial t$, …)

$$u'' = \frac{dF}{dt}|_{t=t_0} = F_t + FF_u \tag{3}$$

$$u''' = \frac{d}{dt}\left(\frac{dF}{dt}\right)|_{t=t_0} = \frac{d}{dt}(F_t + FF_u) = F_{tt} + 2FF_{tu} + F^2F_{uu} + F_tF_u + FF_u^2 \tag{4}$$

because

$$\frac{d}{dt}(F_t) = F_{tt} + F_{tu}\frac{du}{dt} = F_{tt} + FF_{tu} \tag{5}$$

$$\frac{d}{dt}(FF_u) = F_u\frac{dF}{dt} + \mathrm{F}\frac{dFu}{dt} = F_tF_u + FF_u^2 + FF_{ut} + F^2F_{uu} \tag{6}$$

while since

$$F_u\frac{dF}{dt} = (F_t + FF_u)F_u = F_tF_u + FF_u^2 \tag{7}$$

$$F\frac{dFu}{dt} = F\left(F_{ut} + F_{uu}\frac{du}{dt}\right) = F(F_{ut} + F_{uu}F) = FF_{ut} + F^2F_{uu} \tag{8}$$

Note that if $F(u,t)$ is a constant, then, $u'=F(t)$ can be solved simply using a typical Euler forward (finite differencing) scheme.

The unique feature of the RK method (Eq. (2)) is that the Euler forward scheme in time is fixed, while higher-order derivatives are applied to iteratively estimate the function $F(u, t)$ in a more accurate manner. Under the Euler forward scheme framework, each RK iteration improves its local accuracy or local truncation error, as shown in Fig. 1. The difference for finite differencing method is that the derivative is discretized to a finite differencing in time, as shown in (2′), and in space with a finite truncation error.

Assumed that

$$\varphi[t,\ u(t),\ \Delta t] = \sum_{j=1}^{p}\frac{\Delta t^{j-1}}{j!}\ \frac{dF[t,\ u(t)]^{j-1}}{dt^{j-1}} \tag{9}$$

then (2) can be written as

$$u(t_0 + \Delta t) - u(t_0) = \Delta t\ \varphi[t_0,\ u(t_0),\ \Delta t] + O\left(\Delta t^{p+1}\right) \tag{10}$$

Removing the truncation error results in

$$u_1 - u_0 = \Delta t\ \varphi(t_0,\ u_0,\ \Delta t) \tag{11}$$

So, if u_n is known, then

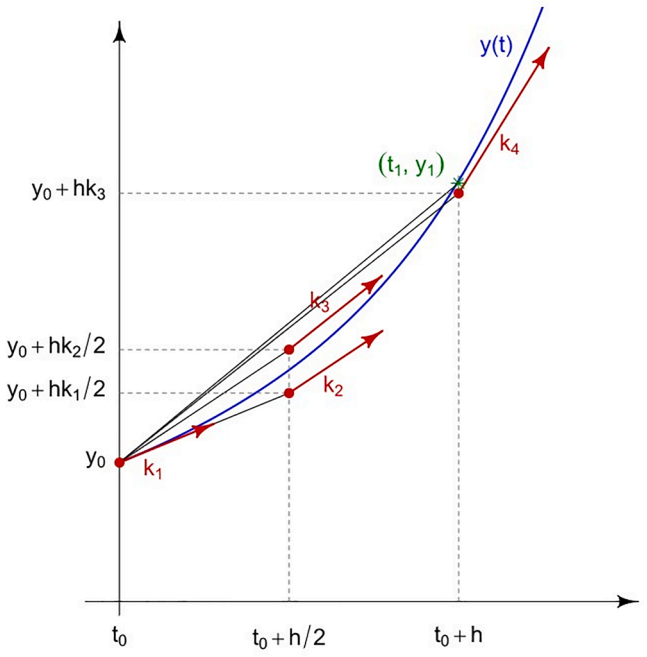

Fig. 1. Slopes used by the classical 3-stage Runge-Kutta method between (t_0, y_0) and (t_1, y_1).

$$u_{n+1} - u_n = \Delta t\ \varphi(t_n,\ u_n,\ \Delta t), \qquad n = 0,\ 1,\ 2,\ \cdots \tag{12}$$

This is the single stepping method with local truncation error (LTE) being $O(\Delta t^{p+1})$ on function φ [i.e., $F(u, t)$]. From (3), (4), and (9), φ based on F's nonlinearity can be estimated. When $p = 1$, it becomes the Euler forward scheme. To calculate $\varphi(t_n, u_n, \Delta t)$, iterative methods are used to estimate φ using higher-order derivatives on $F(u, t)$ based on its initial condition.

In summary, the RK scheme described above is the combination of a 1st-order Euler forward scheme in time and the iterative estimate of higher-order derivative terms of local change in F, which improves the precision (by increasing the local truncation error or local order of accuracy in function $F(u, t)$ on the right hand side). Nevertheless, the global truncation error (GTE) should remain 1st-order accuracy in time, although the local truncation error (LTE) increases with the number of the iterations, or with the stage of the prediction-correction process.

An explicit 2-stage Runge-Kutta scheme, also known as *Heun*'s method (see Durran 2010, p50, Section 2.3.1) is shown below

$$\begin{cases} \xi_1 = \varphi_n \\ \xi_2 = \varphi_n + \Delta t\ F(\xi_1,\ t_n) \\ \varphi_{n+1} = \varphi_n + \dfrac{\Delta t}{2}[F(\xi_1, t_n) + F(\xi_2,\ t_n + \Delta t)] \end{cases} \tag{13}$$

This can be re-written as

$$\begin{cases} (\xi_2 - \xi_1)/\Delta t = F(\xi_1, t_n) \\ (\varphi_{n+1} - \varphi_n)\Big/\Delta t = (\xi_n - \xi_1)\Big/\Delta t = \dfrac{1}{2}\ [F(\xi_1, t_n) + F(\xi_2, t_n + \Delta t)] \end{cases} \tag{14}$$

which is the typical 2-stage predictor-corrector scheme described by Wang and Ikeda (1997a, see Section 2c). This two-stage method, also called the Euler forward-backward scheme, was proved to be weakly inertial unstable by Wang and Ikeda (1997a) and Durran (2010). However, Wang and Ikeda (1997a) proposed a neutral inertially stable scheme for the 2-stage PC scheme, as discussed shortly.

An explicit 3-stage Runge-Kutta scheme, *Heun*'s 3-stage method, can

be written as below [see Durran (2010), chap. 2.3.2, p53],

$$\begin{cases} \xi_1 = \varphi_n \\ \xi_2 = \varphi_n + \dfrac{\Delta t}{3} F(\xi_1, t_n) \\ \xi_3 = \varphi_n + \dfrac{2\Delta t}{3}\ F\left(\xi_2, t_n + \dfrac{\Delta t}{3}\right) \\ \varphi_{n+1} = \varphi_n + \dfrac{\Delta t}{4}\ \left[F(\xi_1, t_n) + 3F\left(\xi_3, t_n + \dfrac{2\Delta t}{3}\right)\right] \end{cases} \tag{15}$$

This formulation can be rewritten following conventional finite differencing format in a PC manner,

$$\begin{cases} (\xi_2 - \xi_1) \Big/ \Delta t\ = \dfrac{1}{3}\ F(\xi_1, t_n) \\ (\xi_3 - \xi_1) \Big/ \Delta t = \dfrac{2}{3} F\left(\xi_2, t_n + \dfrac{\Delta t}{3}\right) \\ (\varphi_{n+1} - \varphi_n) \Big/ \Delta t = (\xi_n - \xi_1) \Big/\ \Delta t = \dfrac{1}{4}\left[F(\xi_1, t_n) + 3F\left(\xi_3, t_n + \dfrac{2\Delta t}{3}\right)\right] \end{cases} \tag{16}$$

where the first two stages are the predictor process, and the last (third) one is the corrector process. Therefore, theoretically and numerically, the *Heun*'s RK3 is a typical 3-stage Euler forward predictor-corrector finite differencing scheme in time (see Appendix A of Wang et al. 2023), although the function $F(\xi_n, t_n)$ on the right-hand side is iteratively updated (i.e., evaluated) at each stage using its higher-order derivatives. Therefore, the RK schemes can be considered structurally similar to the PC family, except for different combination of coefficients. This means that the PC/RK solutions are not unique, depending on the choice of the coefficients.

3. Similarities and differences between the shallow water equations and ODE

For the 2D shallow water equations, or the partial differential equations (PDEs) of the parabolic form, we choose the following form in the rotating system (*f*-plane)

$$\begin{cases} \dfrac{du(x,y,t)}{\partial t} = fv + \mathrm{A_h}\left(\dfrac{\partial^2 u}{\partial x^2} + \dfrac{\partial^2 u}{\partial y^2}\right) \\ \dfrac{dv(x,y,t)}{\partial t} = -fu + \mathrm{A_h}\left(\dfrac{\partial^2 v}{\partial x^2} + \dfrac{\partial^2 v}{\partial y^2}\right) \end{cases} \tag{17}$$

where f is the Coriolis parameter, A_h is the horizontal viscosity coefficient, and the substantial derivative is $\frac{d}{\partial t} = \frac{\partial}{\partial t} + u\frac{\partial}{\partial x} + v\frac{\partial}{\partial y}$, which includes the local time derivative (change) and the non-linear advection term, respectively. This is a typical model for wind-driven circulation.

The partial derivatives of u and v can then be written as,

$$\begin{cases} \dfrac{\partial u}{\partial t} = -\left(u\dfrac{\partial u}{\partial x} + v\dfrac{\partial u}{\partial y}\right) + fv + A_h\left(\dfrac{\partial^2 u}{\partial x^2} + \dfrac{\partial^2 u}{\partial y^2}\right) = \mathrm{Fx}\left(x, y, t, fv, A_h\nabla^2 u, u\dfrac{\partial u}{\partial x} + v\dfrac{\partial u}{\partial y}\right) \\ \dfrac{\partial v}{\partial t} = -\left(u\dfrac{\partial v}{\partial x} + v\dfrac{\partial v}{\partial y}\right) - fu + A_h\left(\dfrac{\partial^2 v}{\partial x^2} + \dfrac{\partial^2 v}{\partial y^2}\right) = \mathrm{Fy}\left(x, y, t, fu, A_h\nabla^2 v, u\dfrac{\partial v}{\partial x} + v\dfrac{\partial v}{\partial y}\right) \end{cases} \tag{18}$$

where $u(x,y,t)$, $v(x,y,t)$ are the functions of x, y, and t. *Fx and Fy* are the "lump sum" of the non-linear terms, Coriolis terms, and viscosity terms $\nabla^2\boldsymbol{u} = \left(\frac{\partial^2 u}{\partial x^2} + \frac{\partial^2 u}{\partial y^2}\right)$, as well as pressure gradient terms and other forcing terms that are not included here. The system is not only the initial problem, but also the boundary problem in the ocean and the atmosphere.

Note that although ODE (1) looks similar to the PDEs (18), they have substantial differences. First, ODE (1), u and $F(u, t)$ are functions of each other, while in PDE (18), u and v are functions of x, y, t, and Fx and Fy on the right hand terms, although the advection terms are "forcefully" included in Fx and Fy. Second, ODE (1) is designed for strongly nonlinear systems, while the advection terms in the ocean and atmosphere are weakly nonlinear because the Rossby number $R_o = U/fL$ [U = 1 (10) m/s, $f = 10^{-4}\ \mathrm{s}^{-1}$, L = 1000 (10,000) km for ocean (atmosphere), R_{o_ocn}=0.01, R_{o_atm}=0.01] is much smaller than 1, with only minor exceptions (e.g. dam breaking in the ocean, and tornados in the atmosphere). Finally, ODE (1) is in a non-rotating, non-viscous system, while the shallow water PDEs (18) are in a rotating, low-viscous system. Therefore, when applying the RK method to weakly nonlinear shallow water PDEs in the rotating system, it should not be taken for granted because potential issues may still need to be addressed.

For example, when applying (3) and (4) (second and third derivatives) to the advection terms of the PDEs ($u\frac{\partial u}{\partial x} + v\frac{\partial u}{\partial y}$ and $u\frac{\partial v}{\partial x} + v\frac{\partial v}{\partial y}$), many additional terms are produced, including cross-derivative terms, and their physical meanings are confusing. Nevertheless, in the leapfrog scheme, the viscosity/diffusion terms are discretized at *n-1* (Wang 1996; Blumberg and Mellor 1987), the dynamical reasoning is that friction kicks off only after the flow velocity (u, v at n) is generated, i.e., physically, friction should lag the advection. In other words, applying RK schemes that are suitable for one variable ODEs to multi-variable PDEs (SWE) seems like using a simple tool to reluctantly solve a complex problem, lacking physical rationale.

Note that Wang (1996) conducted a global linear stability analysis of the complete 2D shallow water equations of Eq. (17) and derived a series of stability criteria including the advection and diffusion Courant-Friedrichs-Lewy (CFL) conditions [see criteria (f) and (a) in the Conclusions on page 1307] using the leapfrog scheme in time and centered differencing in space. Similarly, the explicit Euler-forward RK schemes in Eqs. (13) and (15) must satisfy corresponding necessary stability conditions (Durran 2010, Chapter 2.3 and Fig. 2.4), which, however, do not include the advection and diffusion terms.

4. Analyses of truncation error, numerical viscosity, consistency, and energy conservation

4.1. Analyses of truncation error and numerical viscosity

To show the truncation error in time integration scheme, simplified linear, inertial-diffusion equations are extracted from the shallow water equations:

$$\begin{cases} \dfrac{\partial u}{\partial t} - fv = \mathrm{A_h}\left(\dfrac{\partial^2 u}{\partial x^2} + \dfrac{\partial^2 u}{\partial y^2}\right) \\ \dfrac{\partial v}{\partial t} + fu = \mathrm{A_h}\left(\dfrac{\partial^2 v}{\partial x^2} + \dfrac{\partial^2 v}{\partial y^2}\right) \end{cases} \tag{19}$$

Using the Taylor series expansion,

$$\left\{u^{n+1} = u^n + \frac{\Delta t}{1!}\frac{\partial u}{\partial t} + \frac{\Delta t^2}{2!}\frac{\partial^2 u}{\partial t^2} + O(\Delta t^3)\right. \tag{20}$$

$$\left\{v^{n+1} = v^n + \frac{\Delta t}{1!}\frac{\partial v}{\partial t} + \frac{\Delta t^2}{2!}\frac{\partial^2 v}{\partial t^2}\ + O(\Delta t^3)\right. \tag{21}$$

we have

$$\left\{\frac{\partial u}{\partial t} = \frac{u^{n+1} - u^n}{\Delta t} - \frac{\Delta t}{2!}\frac{\partial^2 u}{\partial t^2}\ + O(\Delta t^2)\right. \tag{22}$$

$$\left\{\frac{\partial v}{\partial t} = \frac{v^{n+1} - v^n}{\Delta t} - \frac{\Delta t}{2!}\frac{\partial^2 v}{\partial t^2}\ + O(\Delta t^2)\right. \tag{23}$$

Note that in most textbooks in numerical methods, this 1st-order

truncation error included in $O(\Delta t)$=$O(-\frac{\Delta t}{2!}\frac{\partial^2 u}{\partial t^2})$ is simply discarded, without looking into what physical processes may be embedded in this truncation error term. In physical oceanography and meteorology, this term may include some important hidden dynamical processes, that are discussed below.

Taking the derivative on u-component of (19) with respect to t gives

$$\frac{\partial^2 u}{\partial t^2} = A_h \frac{\partial}{\partial t}\left(\frac{\partial^2 u}{\partial x^2}+\frac{\partial^2 u}{\partial y^2}\right) + f\frac{\partial v}{\partial t} \tag{24}$$

Then, the truncation error of (22) becomes

$$O(\Delta t) \sim \frac{\Delta t}{2!}\frac{\partial^2 u}{\partial t^2} = \frac{\Delta t}{2!}\left[A_h \frac{\partial}{\partial t}\left(\frac{\partial^2 u}{\partial x^2}+\frac{\partial^2 u}{\partial y^2}\right) + f\frac{\partial v}{\partial t}\right] = \frac{\Delta t}{2!}\left[\boldsymbol{A_h}\nabla^2\frac{\partial u}{\partial t} + f\frac{\partial v}{\partial t}\right] \tag{25}$$

where $\nabla^2 = \left(\frac{\partial^2}{\partial x^2}+\frac{\partial^2}{\partial y^2}\right)$ is the Laplacian operator. Inserting (19) to (25) yields

$$\begin{aligned} O(\Delta t) &\sim \frac{\Delta t}{2!}\frac{\partial^2 u}{\partial t^2} \\ &= -\frac{\Delta t}{2!}\left[A_h\nabla^2\left(-\boldsymbol{fv} + A_h\nabla^2\boldsymbol{u}\right) + \boldsymbol{f}\left(-\boldsymbol{fu} + A_h\nabla^2 v\right)\right] \\ &= \frac{\Delta t}{2!}\left[f\,A_h\nabla^2\boldsymbol{v} + A_h^2\nabla^4\boldsymbol{u} - f^2\boldsymbol{u} + f\,A_h\nabla^2 v\right] \\ &= \frac{\Delta t}{2}\left(A_h^2\nabla^4\boldsymbol{u} + 2\boldsymbol{f}A_h\nabla^2 v - f^2\boldsymbol{u}\right) \end{aligned} \tag{26}$$

Since $f^2 \sim 10^{-8}\ s^{-1} << 1$, the last two terms in (26) can be neglected compared to $-fv$ and $A_h\nabla^2 v$ in (19). Then the truncation error (26) becomes

$$O(\Delta t) \sim \frac{\Delta t}{2!}\frac{\partial^2 u}{\partial t^2} = \frac{\Delta t}{2}A_h^2\nabla^4\boldsymbol{u} \tag{27}$$

In a similar manner of operation, the truncation error of (23) becomes

$$O(\Delta t) \sim \frac{\Delta t}{2!}\frac{\partial^2 v}{\partial t^2} = \frac{\Delta t}{2}A_h^2\nabla^4\boldsymbol{v} \tag{28}$$

Therefore, the 1st-order Euler predictor scheme for the inertial-diffusion system (19) becomes (see also the derivation of Appendix C of Wang et al. 2023):

$$\frac{\mathrm{u}^{n+1*}-\mathrm{u}^n}{\Delta t} - \mathrm{f}v^n = \boldsymbol{A_h}\nabla^2\boldsymbol{u} + \frac{\Delta t}{2}A_h^2\nabla^4\boldsymbol{u} + O(\Delta t^2) \tag{29}$$

$$\frac{\mathrm{v}^{n+1*}-\mathrm{v}^n}{\Delta t} + \mathrm{f}u^n = A_h\,\nabla^2\boldsymbol{v} + \frac{\Delta t}{2}A_h^2\nabla^4\boldsymbol{v} + O(\Delta t^2) \tag{30}$$

as the stage 1 predictor scheme. Note that the last term in (29) and (30) are the bi-harmonic viscosity, which result from the Euler forward finite differencing scheme on the left hand side. The 2–stage corrector process is in a similar way:

$$\frac{\mathrm{u}^{n+1}-\mathrm{u}^n}{\Delta t} - \mathrm{f}\left[\beta\mathrm{v}^{n+1*} + (1-\beta)v^n\right] = \boldsymbol{A_h}\nabla^2\boldsymbol{u} + \frac{\Delta t}{2}A_h^2\nabla^4\boldsymbol{u}, \tag{31}$$

$$\frac{\mathrm{v}^{n+1}-\mathrm{v}^n}{\Delta t} + \mathrm{f}\left[\beta\mathrm{u}^{n+1*} + (1-\beta)\mathrm{u}^n\right] = A_h\,\nabla^2\boldsymbol{v} + \frac{\Delta t}{2}A_h^2\nabla^4\boldsymbol{v}, \tag{32}$$

where $0 \le \beta \le 1$. To obtain neutral inertial stability, $\beta = 0.5 + (f\Delta t)^2/8 \approx 0.50012$ (see Wang and Ikeda 1997a). (29) and (30) can be rewritten as

$$u^{n+1*} = u^n + Fv^n + \Delta t\,A_h\,\nabla^2 u + \frac{\boldsymbol{\Delta t^2}}{2}\mathbf{A_h^2}\nabla^4\boldsymbol{u} \tag{29″}$$

$$v^{n+1*} = v^n - Fu^n + \Delta t\,A_h\,\nabla\,2v + \frac{\boldsymbol{\Delta t^2}}{2}\mathbf{A_h^2}\nabla^4\boldsymbol{v} \tag{30″}$$

Inserting (29′) and (30′) to (31) and (32), respectively, gives

$$\begin{aligned} &\frac{\mathrm{u}^{n+1}-\mathrm{u}^n}{\Delta t} - \mathrm{f}\left\{\beta\left[v^n - Fu^n + \Delta t\,A_h\,\nabla^2 v + \frac{\boldsymbol{\Delta t^2}}{2}A_h^2\nabla^4\boldsymbol{v}\right] + (1-\beta)\mathrm{v}^n\right\} \\ &= \mathrm{A_h}\nabla^2\mathrm{u} + \frac{\Delta t}{2}A_h^2\nabla^4\boldsymbol{u} \end{aligned} \tag{33}$$

$$\begin{aligned} &\frac{\mathrm{v}^{n+1}-\mathrm{v}^n}{\Delta t} + \mathrm{f}\left\{\beta\left[u^n + Fv^n + \Delta t\,A_h\,\nabla^2 u + \frac{\boldsymbol{\Delta t^2}}{2}A_h^2\nabla^4\boldsymbol{u}\right] + (1-\beta)\mathrm{u}^n\right\} \\ &= \mathrm{A_h}\nabla^2\mathrm{v} + \frac{\Delta t}{2}A_h^2\nabla^4\boldsymbol{v} \end{aligned} \tag{34}$$

where $F = f\Delta t$. Further through some algebraic operations, we have

$$\begin{aligned} \frac{\mathrm{u}^{n+1}-\mathrm{u}^n}{\Delta t} - fv^n = A_h\nabla^2 u + \frac{\Delta t}{2}\mathrm{A_h^2}\nabla^4\boldsymbol{u} + \boldsymbol{\beta}\,\boldsymbol{f}\Delta t\,\boldsymbol{A_h}\,\nabla^2\boldsymbol{v} + \frac{\boldsymbol{\beta f\Delta t^2}}{2}\mathrm{A_h^2}\nabla^4\boldsymbol{v} \\ - \boldsymbol{f^2\beta\Delta t u^n} \end{aligned} \tag{33′}$$

$$\begin{aligned} \frac{\mathrm{v}^{n+1}-\mathrm{v}^n}{\Delta t} + fu^n = A_h\nabla^2 v + \frac{\Delta t}{2}\mathrm{A_h^2}\nabla^4\boldsymbol{v} - \boldsymbol{\beta}\,\boldsymbol{f}\Delta t\,\boldsymbol{A_h}\,\nabla^2\boldsymbol{u} - \frac{\boldsymbol{\beta f\Delta t^2}}{2}\mathrm{A_h^2}\nabla^4\boldsymbol{u} \\ - \boldsymbol{f^2\beta\Delta t v^n} \end{aligned} \tag{34′}$$

Since $f = 10^{-4} << 1$ *and* $f^2 << f$, using typical values, A_h=100 $m^2 s^{-1}$, $\Delta t = 10\ s$, $\Delta x = \Delta y = 1\ km = 10^3 m$, $u = 1\ m\ s^{-1}$, then, the scaling analysis shows that the 5 terms on the right-hand side are $O(10^{-4}, 10^{-7}, 10^{-7}, 10^{-10}$, and $10^{-7})$, respectively. After neglecting the terms of $O(10^{-10})$, i.e., $O(\Delta t^2)$, and the last term in comparison to the Coriolis terms on the left-hand side with $O(fu, fv) \sim 10^{-4}$, (33′) and (34′) become

$$\frac{\mathrm{u}^{n+1}-\mathrm{u}^n}{\Delta t} - fv^n \approx A_h\nabla^2 u + \frac{\Delta t}{2}A_h^2\nabla^4\boldsymbol{u} + \boldsymbol{\beta f\Delta t A_h}\nabla^2\boldsymbol{v} + O(\Delta t^2) \tag{35}$$

$$\frac{\mathrm{v}^{n+1}-\mathrm{v}^n}{\Delta t} + fu^n \approx A_h\nabla^2 v + \frac{\Delta t}{2}A_h^2\nabla^4\boldsymbol{v} - \boldsymbol{\beta f\Delta t A_h}\nabla^2\boldsymbol{u} + O(\Delta t^2) \tag{36}$$

The last viscosity terms are produced by the 2nd-stage integration (i.e., corrector process) using the Euler forward scheme of first-order accuracy. Therefore, the 2-stage predictor-corrector scheme is still of 1st-order accuracy in time (global truncation error) with respect to time $O(\Delta t)$. It is noted that the 1-stage Euler forward scheme has the 1st-order accuracy of $\frac{\Delta t}{2}A_h^2\nabla^4\boldsymbol{u}$, and the 2-stage corrector process is also of 1st-order accuracy in time, i.e., $\boldsymbol{\beta f\Delta t A_h}\nabla^2\boldsymbol{v}$. Note that the harmonic viscosity terms in (35) and (36) are asymmetric due to the earth rotation when n-stage PC/RK schemes are applied to the rotating system. In the predictor (stage-1) finite differencing equation, the term $\frac{\Delta t}{2}A_h^2\nabla^4\boldsymbol{u}$ is discarded, i.e., it is not included in the finite differencing scheme, which is equivalent to adding a same, but negative viscosity to the finite differencing schemes. This negative viscosity was found in simulation of the coastal front, which suppresses (sub) mesoscale eddies and weakens the front strength (Schlichting et al. 2024). However, in the corrector finite differencing scheme, $\boldsymbol{\beta f\Delta t A_h}\nabla^2\boldsymbol{v}$ is added back to improve the precision of the predictor process with the missing bi-harmonic viscosity term ($\frac{\Delta t}{2}A_h^2\nabla^4\boldsymbol{u}$). This explains that each of the n-stage Euler forward schemes always improves the **local** precision of its previous (n-1) stage; nevertheless, the global truncation error remains of first-order accuracy in time.

In a similar approach, repeating the same procedure of (29)-(32) easily concludes that the 3- and 4-stage predictor-corrector schemes are also of 1st-order accuracy in time $O(\Delta t)$ with an added viscosity term of 1st-order accuracy. Thus, the higher-stage PC/RK schemes only improve the local accuracy or sub-step truncation error and phase error (as discussed shortly), nevertheless their global truncation errors are still of first-order accuracy in time under the 2-time stepping Euler forward framework.

Note that the truncation errors in (35) and (36) are physically

meaningful because they are horizontal bi-harmonic viscosity terms (the second last terms on the right-hand side) which were generated by the 1st-order Euler forward finite differencing scheme of the left-hand side. The additional viscosity terms (the last terms on the right-hand side) in the finite differencing Eqs. (35) and (36) numerically compensate for the discarded bi-harmonic viscosity. Simply discarding these terms (the second last terms on the right-hand side resulted from the first-order Euler forward scheme) destroys the energy balance in (19), as well as the mass balance in both the temperature and salinity equations (not shown here, but can be easily derived using the same approach; also see Figs. 8–10 of Wang et al. 2023). This is equivalent to removing a true physical process (viscosity) from the SWEs, which would equivalently produce the same "negative viscosity" in the simulated results (Homes et al.2021; Schlichting et al., 2024), effectively dampening (or smoothing) the physical processes, including (sub) mesoscale eddies, front structure, and vertical stratification (see Wang and Ikeda 1997b; Wang et al. 2023; Schlichting et al. 2024). Richardson (1965), a foremost pioneer in numerical weather forecasting from MIT, was perhaps the first scientist (in 1922) making the mistake of using a Euler forward scheme to predict weather in the rotating plane (Kantha and Clayson, 2000, p. 80) and found that the predicted weather was amplified and drifted far away from realistic measurements. This mistake is being made again and again in numerical models more than a century later.

4.2. Consistency of finite differencing scheme with partial differential (shallow water) equations

To examine the consistency of the PC2 finite differencing Eqs. (29)-(32) with the PDE Eqs. (19), particularly in comparison to the leapfrog scheme, we examine the truncation error analysis of the leapfrog scheme performed by Wang et al. (2023, see their Appendix C)

$$\frac{u^{n+1}-u^{n-1}}{2\Delta t}-fv^{n}=A_h\nabla^2\boldsymbol{u}+\frac{\Delta t^2}{6}A_h^3\nabla^6 u \tag{37}$$

$$\frac{v^{n+1}-v^{n-1}}{2\Delta t}+fu^{n}=A_h\nabla^2\boldsymbol{v}+\frac{\Delta t^2}{6}A_h^3\nabla^6 v \tag{38}$$

which is of second-order accuracy $O(\Delta t^2)$. First of all, let us conduct scaling analysis on these two schemes. Setting $\Delta t = 10s$, $\Delta x{=}\Delta y = 1000\ (10^3)m$, $u = v = 1\ (10)\ m/s$, $A_h{=}100\ m^2/s$ in the ocean (atmosphere) models, then we have (with the same unit of ms^{-2})

PC2 : $\frac{\Delta t}{2}\mathbf{A_h^2}\nabla^4\boldsymbol{u}\sim\mathbf{10^{-7}}$ (10^{-10}) and leapfrog: $\frac{\Delta t^2}{6}\mathbf{A_h^3}\nabla^6 u\sim\mathbf{10^{-10}}$ (10^{-14}) for the ocean (atmosphere). Therefore, the truncation error for the leapfrog scheme is three (four) orders of magnitude smaller than the Euler forward PC2 scheme at each time step of the model integration in the ocean (atmospheric) models. Furthermore, the truncation error accumulates over the period of model integration, i.e., the longer the model integrates, the more the error would accumulate. In other words, reducing the time step (Δt) will not reduce the total truncation errors over a constant simulation period.

As for consistency, when Δt approaches (but never equals) 0, the truncation error of the Euler forward PC scheme approaches 0 (i.e., the numerical scheme converges to its PDE) at a rate of Δt, while the leapfrog approaches 0 at a rate of Δt^2. In other words, not only is the truncation error several orders of magnitude smaller for the leapfrog scheme, but it also approaches zero an order of magnitude faster than the Euler forward PC/RK scheme (e.g. Δt = 1, 10^{-1}, 10^{-2}, 10^{-3}…for the Euler forward PC/RK scheme, then the leapfrog scheme approaches 0 at 1, 10^{-2}, 10^{-4}, 10^{-6}…). As such, Euler forward PC schemes of 1st-order accuracy are less consistent with (i.e., slower convergent to) the corresponding PDEs (19) than the leapfrog scheme.

4.3. Energy conservation property of 1st-order Euler forward scheme and leapfrog scheme

Based on the analysis of Wang et al. (2023, see their Appendix D), the following Table 1 can summarize the results.

In a pure advection equation, a scheme with 2nd-order accuracy both in time (leapfrog) and space (centered) conserves energy, because it does not need extra/external viscosity to be stable. A scheme that uses centered differencing in time and 1st-order upwind discretization in space can guarantee a stable physical solution, but includes an undesired, unstable computational mode. By contrast, a scheme with Euler forward discretization in time is unconditionally unstable with either Euler forward (upwind) or centered discretization in space (see also Kantha and Clayson, 2000). In other words, a pure advection system with a 1st-order Euler forward scheme in time needs extra viscosity (and/or diffusion) to be conditionally stable.

The Runge-Kutta scheme is actually in the same family as the Euler forward predictor-corrector scheme of 1st-order accuracy in time. Any 1st-order scheme in time (and in space, not shown here) produces numerical viscosity, preventing energy conservation by adding extra computational (or numerical) dissipation. Therefore, the RK schemes are not energy-conserving, regardless of spatial discretization. To conserve energy, schemes with 2nd-order accuracy in both time and space are essential.

5. Comparison of 3-time stepping schemes

As discussed above, 2-time stepping PC/RK schemes have serious numerical and physical disadvantages, we now investigate three potential 3-time stepping (leapfrog) schemes for improving the truncation error and effectively removing the computational mode. In the following, we examine the leapfrog-trapezoidal, Adams-Bashforth, and leapfrog-hoRA schemes in terms of inertial stability and phase error.

5.1. Leapfrog-trapezoidal (LF-Trap) scheme

The leapfrog scheme with a trapezoidal correction can be written as (see Haidvogel and Beckmann 1999, p64), which is used in the ROMS tracer time integration,

$$\begin{cases} u^{*}=u^{n-1}+2\Delta t U^{n}, \\ u^{n+1}=u^{n}+\dfrac{\Delta t}{2}\left(U^{n}+U^{*}\right) \end{cases} \tag{39}$$

For the inertial wave motion, $U{=}ifu$. Then the LF-Trap scheme can be organized by plugging u^* into the 2nd eq. of (39)

$$\begin{aligned} u^{n+1} &= u^{n}+\frac{\Delta t}{2}\left[ifu^{n}+if\left(u^{n-1}+2\Delta tifu^{n}\right)\right] \\ &= u^{n}+\frac{\Delta t}{2}\left[ifu^{n}+ifu^{n-1}-2\Delta tif^{2}u^{n}\right)] \\ &= \left(1+\frac{\mathrm{if}\Delta t}{2}-\Delta t^{2}f^{2}\right)u^{n}+\frac{\mathrm{if}\Delta t}{2}\,u^{n-1} \end{aligned} \tag{40}$$

Using the same Fourier analysis following Wang et al. (2023), $u^n{=}U0e^{ifn\Delta t}=U_0\,\lambda^n$ ($\lambda{=}\,e^{if\Delta t}$) is inserted into (40), here U_0, f, and Δt are the constant amplitude, inertial frequency, and time step. Then we have the amplification factor (i.e., eigenvalue)

$$\lambda^2+\left(F^2-1-\frac{\mathrm{iF}}{2}\right)\lambda-\frac{\mathrm{iF}}{2}=0 \tag{41}$$

where $F=f\Delta t$. By ignoring terms of order F^2 (since $F{\sim}10^{-3}$ if $\Delta t = 10$ s, $f = 10^{-4}$ s^{-1}), we have the solutions:

Table 1
Stability (eigenvalue λ or the amplification factor, AF) of a pure advection equation/system with four combinations of time and space discretization. The bolded λ indicates a stable scheme.

Amplification factor for a pure advection equation $\frac{\partial u}{\partial t}+\bar{u}\frac{\partial u}{\partial x}=0$	1st-order Euler forward (in time)	2nd-order, centered differencing, leapfrog (in time)
1st-order upwind (in space)	$\lvert\lambda\rvert = 1+\bar{u}\Delta t/\Delta x[1-\cos^2(\alpha\Delta x)] > 1$	$\lvert\lambda_1\rvert = \mathbf{1-2\bar{u}\Delta t/\Delta x[2(1-\cos(\alpha\Delta x))]^{1/2} < 1}$ $\lvert\lambda_2\rvert = 1+2\bar{u}\Delta t/\Delta x[2(1-\cos(\alpha\Delta x))]^{1/2} > 1$
2nd-order, centered (in space)	$\lvert\lambda\rvert = \left\{1+[(2\bar{u}\Delta t/\Delta x)\sin(\alpha\Delta x)]^2\right\}^{1/2} > 1$	$\mathbf{\lvert\lambda_{1,2}\rvert=1}$

$$\lambda_{1,2} \approx \frac{\left(1+\frac{iF}{2}\right)\pm\left(1+\frac{3iF}{2}\right)}{2} \tag{42}$$

$$\left|\lambda_{1,2}\right| \approx \begin{cases} 1+\dfrac{F^2}{2}>1, \\ \dfrac{F^2}{4}\to 0,\ as\ \Delta t\to 0 \end{cases} \tag{43}$$

Although the trapezoidal correction step heavily damps the computational mode as Δt approaches 0, its inertial mode (amplification factor or eigenvalue) is amplifying (Fig. 2), with amplification magnitudes as high as the Euler forward scheme (see Table 2, row 3 with β=0). Therefore, this scheme is unstable for the inertial mode. Note that when this scheme is used in the tracer's time integration of ROMS, there is no Coriolis term in the tracer equation. Thus, no inertial instability exists; nevertheless, the scheme is still the Euler forward scheme of first-order accuracy in time [see eq. (39)], which introduces numerical diffusivity to smooth the temperature and salinity gradients (Schlichting et al., 2024).

The phase error for the physical mode is

$$\omega_1/(-f) = arc\ tan\ [Im(\lambda_1)/Re(\lambda_1)] = [arc\ tan\ (F)]/F \tag{44}$$

which under-estimates the phase speed (Fig. 3).

5.2. Adams-Bashforth (A-B) scheme

The 3-time stepping A-B scheme can be written as (Haidvogel and Beckmann 1999, p59)

$$u^{n+1} = u^n + \Delta t\left(3U^n/2 - U^{n-1}/2\right), \tag{45}$$

where $U^n = U^n(u^n, n\Delta t)$. Using the Fourier analysis (u^n=$U_0\,\lambda^n$), we obtain the eigenvalue (AF), as

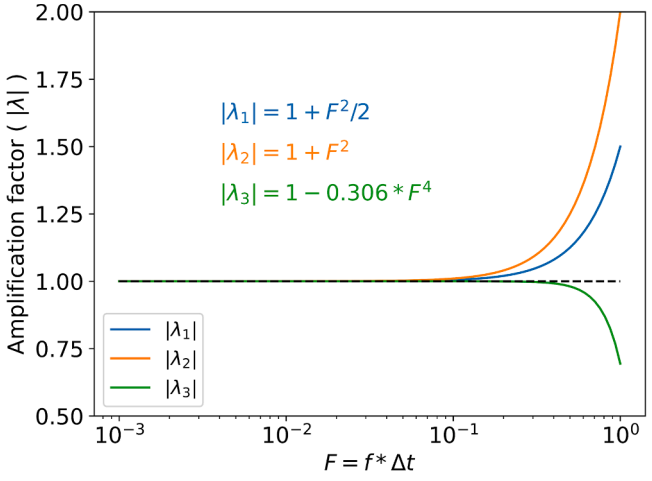

Fig. 2. Amplification factors for 3-time stepping schemes: LF-Trap ($|\lambda_1|$), A-B ($|\lambda_2|$) (both amplifying), and LF-hoRA ($|\lambda_3|$) (slightly damping, nearly neutral).

$$\lambda^2 - (1+i3F/2)\,\lambda - iF/2 = 0 \tag{46}$$

The solutions are

$$\lambda_{1,2} = \frac{1}{2}\left[(1\pm i3F/2) + \sqrt{(1-9F^2/4+iF)}\right] \tag{47}$$

Since $F^2 << F$ ($F = f\Delta t \sim 10^{-3}$), by neglecting the term F^2, we have the following solutions

$$\left|\lambda_{1,2}\right| \approx \begin{cases} 1+F^2>1, \\ F^2\to 0,\ as\ \Delta t\to 0 \end{cases} \tag{48}$$

As seen here, the physical mode λ_1 is as amplifying (see Fig. 2) as the Euler forward scheme (see Table 2, row 3 with β=0), while the computational mode λ_2 is significantly dampened. Therefore, this scheme is unstable.

The phase error for the physical mode is

$$\omega_1/(-f) = arc\ tan\ [Im(\lambda_1)/Re(\lambda_1)] = [arc\ tan\ (F)]/F \tag{49}$$

which is the same as LF-Trap, and under-estimates the phase speed (Fig. 3).

5.3. Leapfrog-hoRA (LF-hoRA) scheme

To achieve both nearly neutral stability and higher order accuracy in amplification factor (at least 2nd-order or higher), Li and Trenchea (2014) proposed a leapfrog scheme with a higher-order Robert-Asselin time filter (LF-hoRA), which can be re-written as

$$\begin{cases} u^{*n+1} = u^{n-1} + 2f\Delta t u^{*n}, \\ u^n = u^{*n} + (\beta/2)\left(u^{*n+1} - 2u^{*n} + u^{n-1}\right) - (\beta/2)\left(u^{*n} - 2u^{n-1} + u^{n-2}\right) \\ \quad = (\beta/2)\left(u^{*n+1} - 3u^{*n} + 3u^{n-1} - u^{n-2}\right) \end{cases} \tag{50}$$

where the dimensionless parameter β is in the interval [0, 1], u^* and u denote the unfiltered and once-filtered values, respectively. Note that $(\beta/2)\,(u^{*n+1} - 3\,u^{*n} + 3u^{n-1} - u^{n-2})$ is a finite differencing approximation to the third time-derivative. The finite differencing approximation of hoRA filter is higher than RAW filter of second time-derivative (Williams 2009) and lower than the fourth time-derivative (Williams 2013).

The finite differencing scheme for LF-hoRA becomes (see Li and Trenchea 2014)

$$u^{n+1} - 2\beta u^n - (1-2\beta)u^{n-1} = iF\left(2u^n - 3\beta u^{n-1} + \beta u^{n-2}\right), \tag{51}$$

or

$$u^{n+1} - 2(\beta+iF)u^n + (i3\beta F - 1 + 2\beta)u^{n-1} - i\beta F u^{n-2} = 0, \tag{51′}$$

Using the same Fourier analysis (Wang et al. 2023), we can obtain the following amplification factor, i.e., eigenvalue λ,

$$\lambda^3 - (\beta+iF)\lambda^2 + (i3F - 1 + 2\beta)\,\lambda - i\beta F = 0, \tag{52}$$

There are three solutions to this scheme, one physical mode, and two computational modes.

When β=0.4, the amplification factor for the physical mode becomes (Li and Trenchea 2014)

Table 2
A summary of inertial stability and phase errors of different time integration schemes for inertial oscillation, $F = f\Delta t$, where f is the Coriolis parameter, and Δt is the time step for model integration.

Time integration scheme	AF, modulus of eigenvalue, $\|\lambda\|$, of inertial motion. β=0, 0.5, and 1 is the Euler forward, centered, and backward scheme, respectively.	Inertial stability feature	Comput. mode?	Normalized phase frequency ω/(-f)=arc tan[Im(λ)/Re(λ)]
3-time stepping, centered differencing, leapfrog (Wang and Ikeda, 1997a)	$\|\lambda_{1,2}\| \equiv 1$	Neutral	Yes	$\omega_{1,2}/(-f) = \frac{\pm 1}{F} arcsinF$; Overestimate
2-time stepping, Euler forward scheme (Wang and Ikeda, 1997a; Durran 2010)	$\|\lambda\| = \begin{cases} (1+F^2)^{\frac{1}{2}} \approx 1+\frac{F^2}{2} > 1, \ if\ \beta = 0 \\ 1, \ if\ \beta = 0.5 \\ (1+F^2)^{-\frac{1}{2}} \approx 1-\frac{F^2}{2} < 1, \ if\ \beta = 1 \end{cases}$	Amplifying/ Unstable Neutral Damping	No	$\frac{\omega}{-f} = \frac{1}{F} arctan\left[\frac{F}{1-\beta(1-\beta)F^2}\right]$; Underestimate
2-time stepping, 2-stage Euler forward PC scheme (Wang and Ikeda, 1997a)	$\|\lambda\| = \begin{cases} \sqrt{1+F^2} \approx 1+\frac{F^2}{2} > 1, \ if\ \beta = 0 \\ \sqrt{1+\frac{F^4}{4}} \approx 1+\frac{F^4}{8} > 1, \ if\ \beta = 0.5 \\ \sqrt{1-F^2+\frac{F^4}{4}} \approx 1-\frac{F^2}{2} < 1, \ if\ \beta = 1 \\ 1, \ if\ \beta = 0.5+\frac{F^2}{8} \end{cases}$	Amplifying/ Unstable Weakly unstable Damping Neutral	No	$\frac{\omega}{-f} = \frac{1}{F} arctan\left(\frac{F}{1-\beta F^2}\right)$; β=0: Underestimate; β=0.5, 1: Overestimate
2-time stepping, 3-stage Euler forward PC scheme (Wang et al. 2023)	$\|\lambda_{1,2}\| = \begin{cases} \sqrt{1+F^2} \approx 1+\frac{1}{2}F^2 > 1, \ \beta = 0 \\ \sqrt{1-\frac{F^4}{4}+\frac{F^6}{16}} \approx 1-\frac{1}{8}F^4 <, \approx 1, \ \beta = 0.5 \\ \sqrt{1-F^2-F^4+F^6} \approx 1-\frac{1}{2}F^2 < 1, \ \beta = 1 \end{cases}$	Amplifying/ unstable Weakly damping /nearly neutral Damping	Yes	$\omega_{1,2}/(-f) = \frac{\mp 1}{F} arctan\frac{F(1-\beta^2F^2)}{1-\beta F^2}$; Underestimate
3-time stepping leapfrog-trapezoidal scheme (Haidvogel and Beckmann 1999) and this study	$\|\lambda_{1,2}\| = \begin{cases} 1+\frac{F^2}{2} > 1, \\ \frac{F^2}{4} \Rightarrow 0, \ as\ \Delta t \Rightarrow 0 \end{cases}$	Amplifying/ Unstable Damping	Yes	$\frac{\omega_1}{-f} = \frac{1}{F} arctanF$ Overestimate, similar to the leapfrog scheme
3-time stepping Adams-Bashforth scheme (Haidvogel and Beckmann 1999) and this study	$\|\lambda_{1,2}\| = \begin{cases} 1+F^2 > 1, \\ F^2 \Rightarrow 0, \ as\ \Delta t \Rightarrow 0 \end{cases}$	Amplifying/ Unstable Damping	Yes	$\frac{\omega_1}{-f} = \frac{1}{F} arctan[F]$ Overestimate, similar to the leapfrog scheme
3-time stepping leapfrog-hoRA scheme (Li and Trenchea 2014) and this study	$\|\lambda_1\|$=1–0.306F^4, when β=0.4	Nearly neutral	Yes	$\frac{\omega_1}{-f} = 1 + 0.024F^4$ Very slightly overestimate, nearly neutral

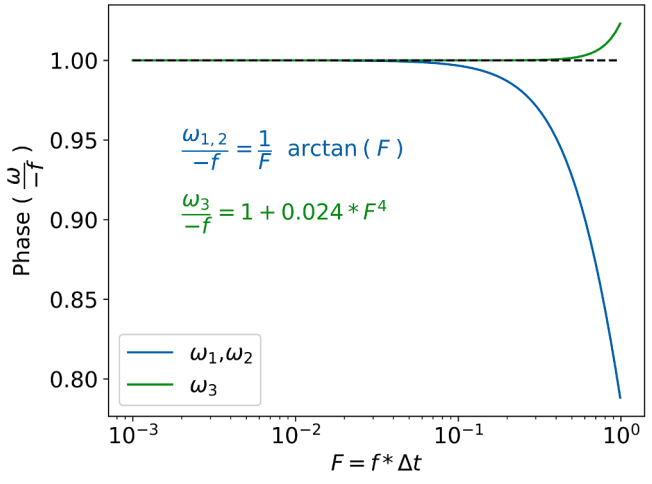

Fig. 3. Phase speed for 3-time stepping schemes: LF-Trap [$\omega_1/(-f)$], A-B [$\omega_2/(-f)$] (under-estimated), and LF-hoRA [$\omega_3/(-f)$] (slightly over-estimated, nearly neutral).

$$|\lambda_1| = 1 - 0.306F^4, \tag{53}$$

and its phase speed is

$$\omega_1/(-f) = 1 + 0.024F^4, \tag{54}$$

Therefore, this scheme is very weakly damping or nearly neutral amplification ($|\lambda_1| \approx 1$, since $0.306F^4 \approx 3.06\times10^{-13} << 1$) (Fig. 2), and the phase speed is very slightly accelerated (Fig. 3); nevertheless it is extremely close to the analytical solution, i.e., $\omega_1/(-f) \approx 1$, since $0.024F^4 \approx 2.4 \times 10^{-2}\times10^{-12} = 2.4 \times 10^{-14} << 1$. In addition, when $F <$ 0.5, the two computational modes are well controlled (see Fig. 2 of Li and Trenchea 2014). Therefore, this LF-hoRA with third-order accuracy in amplification factor is much more accurate than the leapfrog with the RAW filter (Williams 2009, 2013) with second order accuracy in amplification factor (see Table 2 of Li and Trenchea, 2014).

5.4. Inertial stability

Following O'Brien (1986), Wang and Ikeda (1997a), Durran (2010) and Wang et al. (2023), the well-known, simplified, pure inertial oscillation equations (system) are introduced, which are imbedded in both 2D and 3D shallow equations, with no viscosity (or friction) as follows:

$$\begin{cases} \dfrac{\partial u}{\partial t} - fv = 0 \\ \dfrac{\partial v}{\partial t} + fu = 0 \end{cases} \tag{55}$$

The stability for the inertial mode using a variety of finite differencing schemes can be summarized in the following Table 2, taken from Wang et al. (2023), for the sake of easier discussion.

Note that both physical and computational modes in the leapfrog scheme are neutral inertially stable, i.e., neither amplifying nor decaying. Thus, a Robert-Asselin-Williams (RAW) filter is implemented to remove the computational mode. The internal mode of the 1st-order Euler scheme (i.e., β=*0*) has $|\lambda| = \left(1+F^2\right)^{\frac{1}{2}} \approx 1 + F^2/2 > 1$, which is unconditionally inertial unstable. PC2 (i.e., RK2) schemes with β=*0.5* still make the inertial mode very weakly amplifying, where $|\lambda| = \left(1 + \frac{1}{8}F^4\right)/(1 - \frac{1}{8}F^4)$, as shown in the table. However, using $\beta = 0.5 + \frac{F^2}{8} \approx 0.50012$ can force PC2 to be neutrally inertially stable (Wang and Ikeda 1997a). For example, the time integration scheme in MOM6 is the 2-stage RK scheme (RK2 or PC2) with first-order accuracy in time, which is weakly unstable/amplifying in the inertial model if $\beta = 0.5$, but can easily be modified to achieve neutral stability if $\beta = 0.5 + \frac{F^2}{8} \approx 0.50012$.

This analysis of inertial stability also holds true for 3D flows, as demonstrated in Appendix A, and is relevant for all GFD application.

5.5. Phase error between Euler forward PC and leapfrog schemes

We now compare phase error of the Euler forward schemes to the leapfrog scheme in depth. The phase errors for a pure inertial system, as derived in Wang and Ikeda (1997a), Wang et al. (2023), and this study (see Section 5), are summarized in Table 3.

As we see, the Euler forward (leapfrog) scheme underestimates (overestimates) the phase error of *f*-related waves. Nevertheless, the magnitude of the phase error for the 1st-order Euler forward scheme is 33% larger than the leapfrog scheme when Δt is less than 10 s, and the error increases to nearly doubling that of the leapfrog scheme when Δt is 100–1000 s. If the Coriolis terms are not weighted (i.e., with β=0, at the old value), then PC2 and PC3 have the same phase error as PC1, which is larger than leapfrog, in addition to the inertial instability. Therefore, the phase error of the leapfrog scheme is much better than the 1st-order Euler forward scheme.

The phase error for LF-hoRA scheme is three orders of magnitude smaller than any other schemes when Δt is 100–1000 s (Table 3), although slightly overestimated (Fig. 3). This indicates that the phase speed of LP-hoRA scheme is nearly perfectly preserved as the analytical solution (i.e. the true solution is 1). This is in contrast to the phase error of leapfrog and PC2 (over-estimated), and LF-Trap and Addams-Bashforth (under-estimated). Although the phase error of PC3 is slightly better than that of the leapfrog scheme (negative/under-estimated, but ½ magnitude), it still performs significantly worse than LF-hoRA.

6. Conclusions and discussion

In this work, we holistically investigated the nature of the PC/RK schemes from its origin of definition for a nonlinear ODE and compared it to the leapfrog scheme for applications in geophysical fluid dynamics. Then, we differentiated the RK method from the finite differencing scheme. Based on the investigation of truncation error, consistency, numerical viscosity, energy conservation, inertial stability, and phase error, the following conclusions can be drawn.

1) Runge-Kutta schemes belong to the same family as Euler forward predictor-corrector schemes from both mathematical and physical point of view. Both use Euler forward in time and are of 1st-order truncation error (accuracy) in time based on the truncation error analysis. The so-called *n*th-order accuracy in *n*-stage RK (RK*n*) refers to the local truncation error, in which the function terms on the right-hand side of the equation are iteratively evaluated using the *n*th-derivatives, while the 2-time stepping Euler forward differencing scheme is fixed in time integration with *O(Δt)* based on its definition of the Taylor series expansion. The *n*th-stage RK schemes improve only the local truncation error on the function terms, but do not change the nature of the first-order accuracy in time, the global truncation error.
2) Any first-order Euler forward (including n-stage RK/PC) schemes are derived in such a way that they simply discard the first-order term *O(Δt)*. In reality, this term represents physical (bi-harmonic) viscosity, and removing it is equivalent to adding the same, but negative bi-harmonic viscosity back into the numerical model (Schlichting et al., 2024). This negative viscosity destroys the momentum and energy balance of the dynamic system, resulting in indiscriminate damping of all dynamical processes, including vertical stratification, (sub-) mesoscale eddies, and front strength, leading to the drifting in model simulation.
3) Any finite differencing schemes with first-order accuracy in time are less consistent with their original differential equations as Δt approaches zero, in comparison to the 2nd-order leapfrog scheme which is consistent with its PDE. The first-order truncation error in first-order accurate schemes is three orders of magnitude larger than that of the leapfrog scheme. Additionally, as Δt approaches zero, the leapfrog scheme approaches or converges to its PDE with a speed of one order of magnitude faster than typical first-order schemes.
4) In a pure advection system, the amplification factor of any first-order scheme in time and space is always larger than one, leading to nonlinear instability (Table 1). In other words, both Euler forward PC/RK schemes would produce non-linear stability. Thus, an external filter (i.e., numerical viscosity) must be used to dampen the non-linear instability in a model when using PC/RK schemes. This will lead to over-damping/mixing in such a model. It is proved that schemes with at least 2nd-order accuracy in both time and space are required to overcome the nonlinear stability without adding extra/external viscosity.
5) Without weighing the Coriolis terms (i.e., β=0 in Table 2), in addition to inertial instability, the phase error of the 1st-order Euler

Table 3
A summary of the dependence of phase errors of different time integration schemes on time step for inertial oscillation for the 1st-order Euler centered (β=0.0) and 2nd-order centered (leapfrog) differencing schemes: $F = f\Delta t$, where f is the Coriolis parameter (taken 10^{-4} s^{-1}), and Δt (in seconds) is the time step for each model integration. The error is given by the normalized error, $\omega/(-f)$, relative to the true solution, 1, i.e., [$\omega/(-f)$ −1]x100 %. Positive (negative) values indicate the faster (slower) phase speed than the exact solution. Note that the PC2 and PC3 schemes with β=0 are identical to the 1st-order Euler forward scheme.

Δt (s)	F	Euler β=0.0	Leapfrog	PC2 β=0.5	PC3 β=0.5	LF-trap	A-B	LF-hoRA
1	0.0001	-3×10^{-7}	2×10^{-7}	2×10^{-7}	-1×10^{-7}	-2×10^{-7}	-2×10^{-7}	2.4×10^{-16}
10	0.001	-3×10^{-5}	2×10^{-5}	2×10^{-5}	-1×10^{-5}	-2×10^{-5}	-2×10^{-5}	2.4×10^{-12}
100	0.01	−0.00333	0.00167	0.00167	−0.00083	−0.00167	−0.00167	2.4×10^{-8}
1000	0.1	−0.33135	0.16742	0.16616	−0.08259	−0.16742	−0.16742	2.4×10^{-4}
10,000	1	−21.46018	57.07963	10.71487	−1.72063	−57.07963	−57.07963	2.4

forward scheme is twice as large in magnitude as the leapfrog scheme. Equally-weighting the Coriolis terms (β=0.5, see Table 2) also produces a weak inertial instability. After correctly weighing the Coriolis terms (β=0.5 + F^2/8, see Table 2) as we proposed for PC2/RK2, the scheme becomes neutral stable (AF=1). The phase error of PC2/RK2 schemes is as good as leapfrog scheme (twice better than 1st-order Euler forward scheme), and PC3/RK3 is twice better than the leapfrog scheme, i.e., four times better than the Euler forward scheme (see Table 3).

6) It is confirmed that the first-order Euler forward schemes introduce a negative viscosity (Schlichting et al., 2024), seriously dampening and smoothing physical processes; however, with each stage of PC/RK process, a viscosity term associated with the Coriolis (rotation) parameter is added back to the numerical schemes to slightly improve the simulation. As such, the higher the stage, the less damping the physical processes, and the more accurate the amplification factor and phase speed. Nevertheless, the damping/smoothing in model simulations will always exist due to the nature of the first-order truncation error in Euler forward schemes.
7) We compared three schemes with 3-stepping in time: LF-Trapezoidal (LF-Trap), Adam-Bashforth (A-B), and LF-hoRA schemes. We found that although LF-Trap and A-B schemes remove much of the computational mode, the physical mode is amplifying, i.e., inertially unstable, as serious as the Euler forward scheme (β=0, see Table 2). Therefore, we recommend that LF-hoRA scheme be widely used to replace the 2-time stepping PC/RK schemes in ocean modeling, because it possesses nearly neutral inertial stability (Fig. 2 and Table 2) and its phase speed remains very close to the analytical solution (Fig. 3 and Table 2). In addition, the computational modes are well controlled when $F < 0.5$.

Although PC/RK (i.e., Euler forward-backward) methods are widely used to numerically solve non-linear ODEs, there are many major intrinsic shortcomings in the application to PDEs, in particular in the rotating, low-viscous, and strong-stratified ocean. Wang et al. (2023) have proposed and used the leapfrog scheme to replace both the 1st-order Euler forward scheme in the internal mode and RK3 scheme in the external mode of FVCOM. Should RK schemes be used for time integration schemes in ocean (like FVCOM and MOM6) and atmospheric (like WRF) models, we strongly recommend, at the very least, to use the weighted-averaging Coriolis terms (i.e., β=0.5 + F^2/8, see Table 2) to avoid inertial instability and to improve the phase error. Nevertheless, even with the improved inertial stability, Euler forward PC/RK schemes still have intrinsic shortcomings (such as 1st-order accuracy, inconsistency, and lack of energy conservation) in the application to the ocean and atmospheric modeling.

Another issue for the application of RK methods to PDEs is that all the terms, each of which represents a unique physical process (e.g., nonlinear term, gravity wave, inertial mode, viscosity, etc.), are simply "lump-summed" into one term on the right-hand side of the equation at the same time, *n*. This seems awkward because PDEs are solved by discretizing each individual term to its physical need, i.e., with itemized treatment or based on individual dynamical properties. For example, the advection term needs an energy conserving scheme that cannot be achieved by using the 2-time stepping RK schemes; the Coriolis terms should be specially treated with a weighted average (i.e., β=0.5 + F^2/8, see Table 2); and the viscosity term should lag the advection term in time. This kind of lump-summed treatment of PDEs using the 2-time stepping ODE method is an awkward approach in terms of physics and dynamical processes, and should be used cautiously.

While IMplicit-EXplicit (IMEX; Gui et al. 2024) or implicit (Conde et al. 2017) RK schemes have been successfully applied to various PDEs including Landau-Lifshitz equation with arbitrary damping for magnetization dynamics, the schemes introduce even more numerical viscosity (or numerical damping) due to the implicit treatment than the explicit RK schemes (e.g. Heun's 2-stage and 3-stage RK schemes; see Section 2). Thus, these schemes are not suitable to the low-viscous, strong-stratified ocean. The large numerical viscosity of IMEX and implicit RK schemes results not only from the first-order truncation error in time (similar to the explicit RK schemes), but also from the implicit (forward) treatment of the terms including the viscosity term.

If the 1st-order schemes, including PC/RK, must be used, we recommend a remedy that the discarded bi-harmonic viscosity terms ($\frac{\Delta t}{2}A_h^2\nabla^4\boldsymbol{u}$ which is equivalent to a 9-point filter) be added back to the finite differencing equation. When this is done, the truncation error becomes second order and consistency between the numerical scheme and physical properties of the system can be maintained, preserving the integrity of the dynamical system in the discretized scheme. A very popular approach to deal with model drifting away from observations, a symptom of inaccurate physical representations and unstable or over-mixing schemes, is so-called "bias correction." This is a simple data nudging which "forcefully" brings a drifting model back to the measurement, regardless of errors resulting from numerical schemes, mixing schemes, and/or other improper parameterizations. As stated above, this bias correction seems to treat the symptoms, rather than the disease.

Although not perfect, the leapfrog scheme, nevertheless, has been widely used in ocean and atmospheric models because it holistically possesses the following important mathematical and physical properties: 1) 2nd-order accuracy, 2) introduces no numerical viscosity, 3) consistency to its PDE, 4) neutral inertial stability and minimal phase error, and 5) energy conservation. The major shortcoming is that the leapfrog scheme introduces a computational mode, which is also introduced by the PC3/RK3 and PC4/RK4 schemes (Wang et al. 2023). The other major shortcoming is overshooting or oscillatory features when it is applied to a pure advection scheme with a step-like function [see Eq. (25) and Figs. 3-6 of Durran (1991)]. Nevertheless, in ocean dynamics and thermodynamics, there are no such step-like functions for temperature, salinity, and ocean velocity. For example, at a river mouth or estuary connecting to the ocean, no zero salinity is ever observed next to the coastal ocean (say with 25 PSU, pratical salinity unit). Another example is that even in the case of strong vertical stratification in the Arctic, the thermohaline layer always has smooth transition, rather than the step-like transition. Strong horizontal and vertical velocity shears along the strongest currents, the Kuroshio and the Gulf Stream, always have smooth gradient. There are no such velocity gradient changing from 0 ms^{-1} at one grid to 1 ms^{-1} at the next surrounding grids in both realistic measurements and model simulations. Therefore, the step-like function used to test the pure advection equation may be ill-posed for ocean temperature, salinity, and velocity. Both computational mode and oscillatory behavior in the leapfrog scheme can be easily controlled or minimized by the LF-hoRA filter (Williams, 2009, 2013; Li and Trenchea, 2014).

It should be pointed out that when applying a novel computational method developed in computational and applied mathematics (such as implicit-explicit and implicit RK schemes with large damping) to ocean and atmospheric modeling, the above mentioned five physical properties should be used as criteria to gauge the suitability. A novel, efficient scheme in computational mathematics or other research fields is not necessarily a suitable scheme to GFD, because it may not fit the rotational, low-viscous, and strong-stratified ocean. Therefore, before the application, stability criteria derived in such novel, efficient schemes in a non-rotating, high-viscous, and non-stratified system should be holistically re-examined in the rotating, low-viscous, and strong-stratified ocean and atmospheric systems.

CRediT authorship contribution statement

Jia Wang: Writing – original draft, Funding acquisition, Conceptualization. **David Cannon:** Writing – review & editing, Investigation. **Yang Song:** Writing – review & editing, Methodology. **Haoguo Hu:** Methodology, Formal analysis. **Ayumi Fujisaki-Manome:** Writing –

review & editing, Investigation. **Andrea VanderWoude:** Writing – review & editing, Validation. **Oliver Fringer:** Writing – review & editing, Conceptualization.

Declaration of competing interest

The authors declare the following financial interests/personal relationships which may be considered as potential competing interests:

Jia Wang reports financial support was provided by NOAA Great Lakes Environmental Research Laboratory. Jia Wang reports a relationship with National Oceanic and Atmospheric Administration that includes: employment. No If there are other authors, they declare that they have no known competing financial interests or personal relationships that could have appeared to influence the work reported in this paper.

Acknowledgements

The study was supported by NOAA OAR Ocean Science Portfolio project entitled "Great Lakes Earth System Model" and NOAA GOMO Arctic Research Program, awarded to JW. The authors would like to thank Dr. Alisa Young of GLERL for editing this paper. This is GLERL Contribution No. 2097 and CIGLR Contribution No. 1278.

Appendix A: Inertial stability in 3D stratified, shear flows

We have discussed the inertial stability of 2D shallow water equations in Section 5.4. A question may be asked: can the inertial stability (Table 2) be applied to 3D shear flow? In the next step we will confirm that the theoretical problem is a real problem in the 3D shear flow. This should be observable in the following simplified case that features only the influence of the Coriolis term, with no other wave motion.

A stable shear layer on a doubly-periodic *f*-plane should suffice. There, in a domain of depth 1 ($-1 \le z \le 0$), one could have:

$$\begin{cases} u(t=0) = \alpha(z+1/2), \\ v(t=0) = 0, \\ T = T_0 + \theta z, \end{cases} \tag{A1}$$

(see Fig. A1) such that the Richardson number is safely above 1 (suppressing any shear instability), the baroclinic state is constant, and the Coriolis force applies only to the shear layer without inducing wave motion. Here α, θ are both positive constants. If this case is unstable, then the 3D fluid clearly has inertial instability.

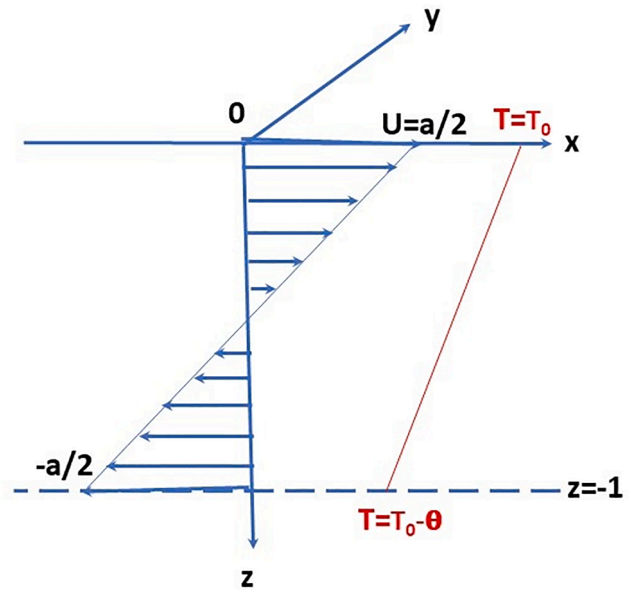

Fig. A1. 3D shear flow with vertical (linear) stratification.

This is a quasi-3D problem with horizontally (y) homogeneous distribution in T, u and v, and vertically linear distribution in T (temperature stratification) and v (velocity shear) (Fig. 2). So, the 3D equations become, by ignoring advection terms, density forcing, gravity waves, and wind forcing,

$$\begin{cases} \dfrac{\partial u}{\partial t} - fv = \mathbf{A}_z \dfrac{\partial^2 u}{\partial z^2} \\ \dfrac{\partial v}{\partial t} + fu = \mathbf{A}_z \dfrac{\partial^2 v}{\partial z^2} \\ \dfrac{\partial T}{\partial t} = \mathbf{K}_z \dfrac{\partial^2 T}{\partial z^2} \end{cases} \tag{A2}$$

Inserting (A1) into (A2) yields

$$\frac{\partial u}{\partial t} - fv = \mathbf{A}_z \frac{\partial^2 u}{\partial z^2} = 0$$
$$\frac{\partial v}{\partial t} + fu = \mathbf{A}_z \frac{\partial^2 v}{\partial z^2} = 0 \quad \text{(A3)}$$
$$\frac{\partial T}{\partial t} = \mathbf{K}_z \frac{\partial^2 T}{\partial z^2} = 0$$

Then this 3D system degrades into the 2-D pure inertial motion system (39) that is used for theoretical stability analysis. Therefore, all the theoretical results derived from (39) apply to 3D shear flow with stratification. The physical meaning behind this is that as long as a 2D (barotropic) inertial system is inertially unstable, its 3D (stratified) system must be unstable, because the 3D system consists of n (vertical) layers of 2D systems. This is why stability analysis is usually conducted in the 2D shallow water equations (Wang 1996).

Data availability

No data was used for the research described in the article.

References

Bai, X., Wang, J., Schwab, D.J., Yang, Y., Luo, L., Leshkevich, G.A., Liu, S., 2013. Modeling 1993-2008 climatology of seasonal general circulation and thermal structure in the Great Lakes using FVCOM. Ocean Model. 65, 40–63. https://doi.org/10.1016/j.ocemod.2013.02.003.

Beckers, J.-M., 1999. On some stability properties of the discretization of damped propagation of shallow-water inertia-gravity waves on Arakawa B-grid. Ocean Model. 53–69.

Beckers, J.-M., Deleersnijder, E., 1993. Stability of a FBTCS scheme applied to the propagation of shallow-water inertia-gravity waves on various space grids. J. Comput. Phys. 108 (1), 95–104.

Blumberg, A.F., Mellor, G.L., 1987. A description of 3-D coastal ocean circulation model. p 1–16. In: Heaps, N.S. (Ed.), Coastal and Estuarine Sciences 4: 3-D Coastal Ocean Models. American Geophysical Union, Washington, D.C.

Bruyère, C.L., Done, J.M., Holland, G.J., Fredrick, S., 2014. Bias corrections of global models for regional climate simulations of high-impact weather. Clim. Dyn. 43, 1847–1856. https://doi.org/10.1007/s00382-013-2011-6, 2014.

Cannon, D.A., Fujisaki-Manome, J., Wang, J., Kessler, Chu, P., 2023. Modeling changes in ice dynamics and subsurface thermal structure in Lake Michigan-Huron between 1979 –2021. Ocean. Dyn. https://doi.org/10.1007/s10236-023-01544-0.

Cannon .A., D., Wang, J., Fujisaki-Manome, A., Kessler, J., Ruberg, Steve, Constant, Steve, 2024. Investigating multidecadal trends in ice cover and subsurface temperatures in the Laurentian Great Lakes using FVCOM+CICE models. J. Clim. 37, 1249–1276. https://doi.org/10.1175/JCLI-d-23-0092.1.

Chen C., R.C. Beardsley, G. Cowles, J. Qi, Z. Lai, G. Gao, D. Stuebe, Q. Xu, P. Xue, J. Ge, S. Hu, R. Ji, R. Tian, H. Huang, L. Wu, H. Lin, Y. Sun, and L. Zhao, 2013. An Unstructured Grid, Finite-Volume Community Ocean Model FVCOM User Manual, Tech. Rep., SMAST/UMASSD-13-0701, 4th ed, 416 pp., Sch, Mar, Sci, Technol, Univ, Mass, Dartm. New Bedford.

Chelton, D.B., DeSzoeke, R.A., Schlax, M.G., 1998. Geographical variability of the first baroclinic Rossby radius of deformation. J. Phys. Ocean. 28, 433–460.

Conde, S., Gottlieb, S., Grant, Z.J., Shadid, J.N., 2017. Implicit and implicit-explicit strong stability preserving Runge-Kutta methods with high linear order. J. Sci. Comput 73, 667–697.

Dosio, A., Paruolo, P., 2011. Bias correction of the ENSEMBLES high-resolution climate change projections for use by impact models: evaluation on the present climate. J. Geophys. Res.-Atmos. 116, D16106. https://doi.org/10.1029/2011JD015934.

Durran, D.R., 1991. The third-order Adams-Bashforth method: an attractive alternative to leapfrog time differencing. Mon. Wea. Rev. 119, 702–720.

Durran, D.R., 2010. Numerical Methods for Fluid Dynamics with Application to Geophysics, 2nd Edition. Springer, New York, p. 516.

Gill, A.E., 1982. Atmosphere-Ocean Dynamics. Academic Press.

Gui, Y.C., Wang, Chen, J., 2024. IMEX-RK methods for Landau-Lifshitz equation with arbitrary damping. Commun. Math. Sci. 22 (5), 1397–1425.

Haidvogel, D.B., Beckmann, A., 1999. Numerical Ocean Circulation Modeling. Imperial College Pree, p. 320pp.

Holmes, R.M., Zika, J.D., Griffies, S.M., Hogg, A.M., Kiss, A.E., England, M.H., 2021. The geography of numerical mixing in a suite of global ocean models. J. Adv. Model. Earth Syst. 13, e2020MS002333. https://doi.org/10.1029/2020MS002333.

Holton, J.R., 1979. An Introduction to Dynamic Meteorology, 2nd Edition. Academic Press, p. 391.

Hutson, A., Fujisaki-Manome, A., Lofgren, B., 2024. Testing the sensitivity of a WRF-based great lakes regional climate model to cumulus parameterization and spectral nudging. J. Hydrometeorol. 25, 1007–1025.

Kantha, L.H., Clayson, C.A., 2000. Numerical Models of Oceans and Ocean Processes. Academic Press, New York, p. 936.

Klingbeil, K., Mohammadi-Aragh, M., Gräwe, U., Burchard, H., 2014. Quantification of spurious dissipation and mixing – discrete variance decay in a finite-volume framework. Ocean Model. 81 (2014), 49–64.

Li, R.-H., Feng, G.-S., 1990. Numerical methods to differential equations. High Education Publisher, China, p. 348. (in Chinese).

Li, Y., Trenchea, C., 2014. A higher-order Robert-Asselin type time filter. J. Comput. Phys. 259, 23–32.

Nurser, A.J.G., Bacon, S., 2014. The Rossby radius in the Arctic Ocean. Ocean Sci. 10, 967–975. https://doi.org/10.5194/os-10-967-2014.

O'Brien, J.J., 1986. Time integration schemes. In: O'Brien, J.J. (Ed.), Advanced Physical Oceanographic Numerical Modelling. Reidel Publishing Company, Boston, pp. 155–163. NATO ASI Series.

Richardson, L.F., 1965. Weather Prediction by Numerical Process. Dover, New York, p. 236.

Pedlosky, J., 1979. Geophysical Fluid Dynamics. Springer-Verlag, New York, p. 723.

Schlichting, D., Hetland, R., Jones, C.S., 2024. Numerical mixing suppresses submesoscale baroclinic instabilities over sloping bathymetry. J. Adv. Model. Earth Syst. 16, e2024MS004321. https://doi.org/10.1029/2024MS004321.

Shchepetkin, A.F., McWilliams, J.C., 2009. Computational kernel algorithms for fine-scale, multi-process, longtime oceanic simulations. In: Handbook of Numerical Analysis, 14. Elsevier, pp. 121–183. https://doi.org/10.1016/S1570-8659(08)01202-0.

Skamarock, W.C., Klemp, J.B., Dudhia, J., Gill, D.O., Liu, Z., Berner, J., Wang, W., Powers, J.G., Duda, M.G., Barker, D.M., 2019. A Description of the Advanced Research WRF Model Version 4. Natl. Cent. Atmos. Res. 145, 145. https://opensky.ucar.edu/islandora/object/technotes%3A588.

Wang, J., 1996. Global linear stability of the 2-D shallow water equations: an application of the distributive theorem of roots for polynomials on the unit circle. Mon. Wea. Rev. 124 (6), 1301–1310.

Wang, J., Ikeda, M., 1997a. Inertial stability and phase error of time integration schemes in ocean general circulation models. Mon. Wea. Rev. 125 (9), 2316–2327.

Wang, J., Ikeda, M., 1997b. Diagnosing ocean unstable baroclinic waves and meanders using quasi-geostrophic equations and Q-vector method. J. Phys. Ocean. 27 (6), 1158–1172.

Wang, J., Manome, A., Kessler, J., Cannon, D., Chu, P., 2023. Inertial instability and phase error in Euler forward predictor-corrector time integration schemes: application to the improvement of modeling thermal structure and circulation in the Great Lakes. Ocean Dyn. https://doi.org/10.1007/s10236-023-01558-8.

Wicker, L.J., Skamarock, W.C., 2002. Time-splitting methods for elastic models using forward time schemes. Mon. Wea. Rev. 130, 2088–2097.

Williams, P.D., 2009. A proposed modification to the Robert-Asselin filter. Mon. Weather Rev. 137, 2538–2546.

Williams, P.D., 2013. Achieving seventh-order amplitude accuracy in leapfrog integrations. Mon. Wea. Rev. 141, 3037–3050.

Zobel, Z., Wang, J., Wuebbles, D.J., Kotamarthi, V.R., 2018. Analyses for high-resolution projections through the end of the 21st century for precipitation extremes over the United States. Earth's Future. https://doi.org/10.1029/2018EF000956.